Synthesis and Characterization of MnO_2 Nanoparticle Composite and Palm Kernel Shell-Based Activated Carbon as Supercapacitor Electrode Candidates

Ainun Rezkiva Arif[1], Muhammad Zakir[1*], Ahyar Ahmad[1,2], Indah Raya[1], Paulina Taba[1], and Herlina Rasyid[1]

[1]*Department of Chemistry, Faculty of Mathematics and Natural Sciences, Hasanuddin University, Jl. Perintis Kemerdekaan Km. 10, Makassar 90245, Indonesia*

[2]*Research and Development Center for Biopolymer and Bioproducts, LPPM, Hasanuddin University, Jl. Perintis Kemerdekaan Km. 10, Makassar,90245 Indonesia*

* ***Corresponding author:***

tel: +62-81341945533
email: muh.zakir@science.unhas.ac.id

Received: August 29, 2025
Accepted: October 24, 2025

DOI: 10.22146/ijc.110797

Abstract: *Palm kernel shells (PKS) are a biomass waste rich in carbon and low in ash content, making them suitable for conversion into supercapacitor electrode materials that support the principles of the blue economy and green technology. This study presents a novel synthesis approach for supercapacitor electrode materials by combining activated carbon derived from hydrothermally carbonized PKS biomass waste (AC-PKS) with MnO_2 nanoparticles. Carbon activation in this study was carried out using chemical and physical activation approaches to produce a microporous structure with a high surface area. The AC-PKS/MnO_2 composite was then synthesized through a redox reaction deposition using $KMnO_4$ to create materials that exhibit potential properties between double-layer capacitance and pseudocapacitive behavior. Electrochemical testing with CV and GCD showed an increase in the specific capacitance of the AC-PKS/MnO_2 composite of 67.85 and 46.91 F/g, respectively. These findings indicate the scientific contribution of combining biomass-derived activated carbon with metal oxides as a potential supercapacitor electrode. The implications of these results suggest that AC-PKS/MnO_2 not only offers a sustainable material solution but also opens up opportunities for the development of high-capacity supercapacitor electrodes for future energy storage applications, particularly in renewable energy and environmentally friendly technologies.*

Keywords: *activated carbon; composite materials; nanoparticle; palm shell; supercapacitor*

■ INTRODUCTION

The quest for sustainable, environmentally friendly, and relevant energy sources in the modern era has driven humans to strive harder for efficient and high-performance energy storage technologies [1]. Energy storage is crucial for maintaining a stable and reliable electricity grid, as electricity is a fundamental necessity in modern life [2]. One energy storage technology that can store large amounts of energy and is environmentally friendly is the supercapacitor [3]. Supercapacitors are a promising solution for sustainable energy storage systems due to their quick charging and discharging rates, long durability, high capacitance values, and high-power density [4].

The performance of a supercapacitor is affected by the material used for the electrodes and the electrolytes [5]. The electrode materials are crucial in enhancing the performance of supercapacitors and are categorized into three types: carbon-based materials, polymer conductors, and metal oxides [2]. Currently, metal oxide composites and activated carbon (AC) are very popular topics for material development as energy storage materials. Metal oxides are often utilized in supercapacitor applications due to their excellent electrochemical stability and high energy density [5].

Manganese dioxide (MnO_2) is a metal oxide that has the potential as a supercapacitor electrode material

because it has a high specific capacitance of around 1370 F/g, is environmentally friendly, non-toxic, and low-cost [6-7]. However, MnO_2 has a weakness in low electrical conductivity, so it needs to be composited to improve its electrochemical performance [8-9]. To overcome this limitation, MnO_2 can be composited with carbon-based materials.

One material that can support the electrochemical performance of MnO_2 is AC, as it has a large surface area, adjustable porosity, and good surface reactivity [10]. One type of biomass waste that can be used as AC is palm kernel shell (PKS), as it is abundant in nature, easily obtainable, contains high lignocellulose content, has low ash content, and produces a significant amount of AC [11-12]. The high carbon content in PKS can be used as a valuable resource, especially for conversion into porous carbon [13]. A suitable method for producing a large surface area is hydrothermal carbonization, as it is an environmentally friendly process that can be applied in energy storage [14]. Additionally, the hydrothermal carbonization method can also produce nanomaterials easily and quickly with high purity in a relatively short time [15]. MnO_2 and AC composites synergistically provide good electrochemical performance due to the high pseudocapacitance of MnO_2 and the exceptional electrical conductivity of AC [16]. Additionally, the morphology and distribution of MnO_2 on the surface of AC also play a role in determining the electrochemical characteristics of the composite [17-18].

Research on AC and MnO_2 composites has been extensively studied using various carbon-based materials, including AC derived from acacia wood [16], eggplants, peanut shells [19], coconut shells [20], and commercial AC [17]. In this study, the biomass waste used was PKS obtained from a palm oil plantation in Bontang City, Kalimantan Timur, Indonesia. PKS were used as AC in this study because they have a low ash content. Additionally, this was done to enhance the sustainability aspects of the blue economy approach and increase the value of PKS, which are commonly used only as boiler fuel.

The novelty of this research lies in the hydrothermal carbonization method and the gradual chemical and physical activation process. The use of hydrothermal carbonization in this study is not only a technical choice but also a strategic approach to forming initial carbon structures in a more targeted manner within an aqueous environment at moderate temperatures. This process enables the formation of a stable aromatic carbon framework while retaining functional oxygen groups that play an essential role in electrochemical interactions. The uniqueness of this method lies in its ability to trigger pore formation from an early stage, which is then selectively expanded through chemical activation using KOH, followed by physical activation at high temperatures. This combination of gradual activation is expected to produce AC with a high surface area and pore structure, suitable for charge storage in supercapacitors. A further method involved depositing MnO_2 on the surface of AC through reduction with $KMnO_4$, resulting in an effective and efficient supercapacitor electrode material due to the Mn^{4+}/Mn^{3+} redox system, which enables the pseudocapacitive process of MnO_2 with electron transfer, thereby facilitating charge storage. This study is a preliminary investigation to evaluate the potential of composite materials made from AC derived from PKS and MnO_2, to identify their suitability as supercapacitor electrodes through the synergistic interaction between the microporous structure of carbon and the redox activity of MnO_2, which can be used to store energy in the future and increase the value of biomass waste for a blue economy approach.

■ EXPERIMENTAL SECTION

Materials

The primary material used in this study was PKS obtained from Bontang City, East Kalimantan, Indonesia. The chemicals used for the synthesis of AC and nanoparticle composites in this study were KOH (99.9%, Merck, Germany) and $KMnO_4$ (99.9%, Merck, Germany). The electrodes were made using carbon black from Super P and polyvinyl alcohol from Merck (Germany) with 88% hydrolysis. H_2SO_4 from Merck (Germany) was used as the electrolyte in electrochemical testing. Supporting materials used in this study included

distilled water, Whatman No. 42 filter paper, and universal pH paper.

Instrumentation

The instruments employed in this research included a UV-vis spectrophotometer (T60-spectroscopy) for analyzing the reduction process from the composite. The elemental composition and morphology were analyzed using a scanning electron microscope combined with energy-dispersive X-ray spectroscopy (SEM-EDX) on the HITACHI SU3500 imaging system. Pore distribution and surface area were analyzed using a surface area analyzer (SAA) on the Micro-200 system. The crystallinity and phase characteristics were examined through X-ray diffraction analysis (XRD) performed using the Shimadzu 7000 Maxima system. Functional groups and chemical structure were analyzed using Fourier-transform infrared (FTIR) spectroscopy with the Prestige-21 system.

Procedure

Synthesis of AC-PKS

PKS are cleaned using distilled water to remove surface impurities that can interfere with the carbonization process, then dried in the sun for 3 days to reduce the water content. The PKS is then ground into a fine powder to increase the surface area available for contact during the synthesis process. A total of 15 g of PKS powder was mixed with 75 mL of distilled water (1:5) and processed in a Teflon-coated autoclave at 200 °C for 4 h, where this temperature and duration were selected to facilitate initial thermal decomposition and were a modification of the study by Nakason et al. [20]. After cooling and filtering, the sample was dried at 100 °C for 2 h to remove the moisture content in the hydrochar. Chemical activation was performed using a 3 M KOH solution with a mass ratio of 1:5, which was empirically known to be effective in opening pores and increasing the surface area of the carbon. The stirring process lasted for 1 h, and the soaking process lasted for 24 h, allowing the activator solution to penetrate the carbon matrix evenly. Physical activation was then carried out at a temperature of 700 °C for 2 h, which is the optimal temperature for developing a pore structure without causing sintering. The activation process was carried out based on the modifications and optimal conditions described by Li et al. [21]. After physical activation, washing is performed until the pH is neutral, yielding activated carbon (AC-PKS).

Synthesis of AC-PKS/MnO_2

The synthesis of AC-PKS/MnO_2 composite was carried out through a reduction reaction between a $KMnO_4$ solution and AC-PKS, where AC-PKS served as the reducing agent. A total of 2 g of AC-PKS, which had been meshed to a 200-mesh size, was placed in an Erlenmeyer flask to ensure an optimal contact surface area during the reaction. Then, 100 mL of 0.03 M $KMnO_4$ solution was added, which was selected and modified based on research conducted by Thuy et al. [22]. The mixture was shaken at room temperature for a sufficient time to ensure homogenization and contact between particles, as indicated by a color change from purple to light brown, which served as a visual indicator of the reduction of Mn^{7+} to Mn^{4+}. After the reaction was complete, the solution was filtered and analyzed using a UV-vis spectrophotometer to confirm the presence of MnO_2. The reaction precipitate was then thoroughly rinsed to remove residual ions and dried at 60 °C for 12 h. This temperature was chosen to avoid degradation of the MnO_2 structure while ensuring complete evaporation of water [16]. The resulting composite was labeled AC-PKS/MnO_2.

Electrode fabrication and measurement

The electrodes were made by inserting copper wire into a pipette and then sealing it with parafilm. AC-PKS and AC-PKS/MnO_2 were mixed with carbon black and polyvinyl alcohol at a mass ratio of 80:10:10 (wt.%) and stirred until a homogeneous mixture was achieved. A paste was then formed using a spatula in a petri dish. Then, to ensure the carbon paste is evenly spread and compact, it is pushed into the electrode body with a spatula. The finished electrodes are then dried at 60 °C for 2 h before testing [19].

The weight of the active material loaded on each electrode is approximately 50 mg. Electrochemical measurements were performed using cyclic voltammetry (CV), galvanostatic charge-discharge (GCD), and electrochemical impedance spectroscopy

(EIS) on an EA161 potentiostat with a three-electrode system consisting of a platinum (Pt) working electrode, an Ag/AgCl reference electrode, and a counter electrode. Electrochemical testing was carried out in a 1 M H_2SO_4 electrolyte solution. The specific capacitance of the working electrode was calculated from the CV curve using Eq. (1) [23];

$$C_s = \frac{\int idV}{2km\Delta V} \quad (1)$$

where C_s is the specific capacitance (F/g), k is the scan rate (mV/s), m is the active mass of the electrode (g), ΔV is the potential window (V), and ∫idV the area under the CV curve.

In addition, the working electrode measured with GCD can be calculated for specific capacitance, specific energy, and specific power using Eq. (2–4) [21];

$$C_{sc} = \frac{I \times \Delta t}{m \times \Delta V} \quad (2)$$

$$E_{sc} = \frac{C_{sc} \times \Delta V^2}{2 \times 3.6} \quad (3)$$

$$P_{sc} = \frac{3600 \times E_{sc}}{\Delta t} \quad (4)$$

where C_{sc} is the specific capacitance (F/g), E_{sc} is the energy density (Wh/kg), P_{sc} is the power density (W/kg), I is the charge-discharge current (A), m is the total mass of active material (g), Δt is the discharge time (s), and ΔV is the potential window (V).

■ RESULTS AND DISCUSSION

Morphology, Elemental Composition, and Surface Area Analysis

The morphological structure and elemental composition of AC-PKS and AC-PKS/MnO_2 are depicted in Fig. 1. The morphological structure of the chemically and physically AC-PKS is shown in Fig. 1(a). The morphology of AC-PKS reveals that the particles appear granular, with numerous gaps between them. Choi et al. [24] conducted similar research and produced an AC with a smooth surface and irregular cut shapes. Research conducted by Pam et al. [12] obtained the AC surface morphology of PKS with open pores due to activation using H_3PO_4. The activation process results in the formation of micropore and mesopore structures, causing the pores to be arranged and compressed. As explained

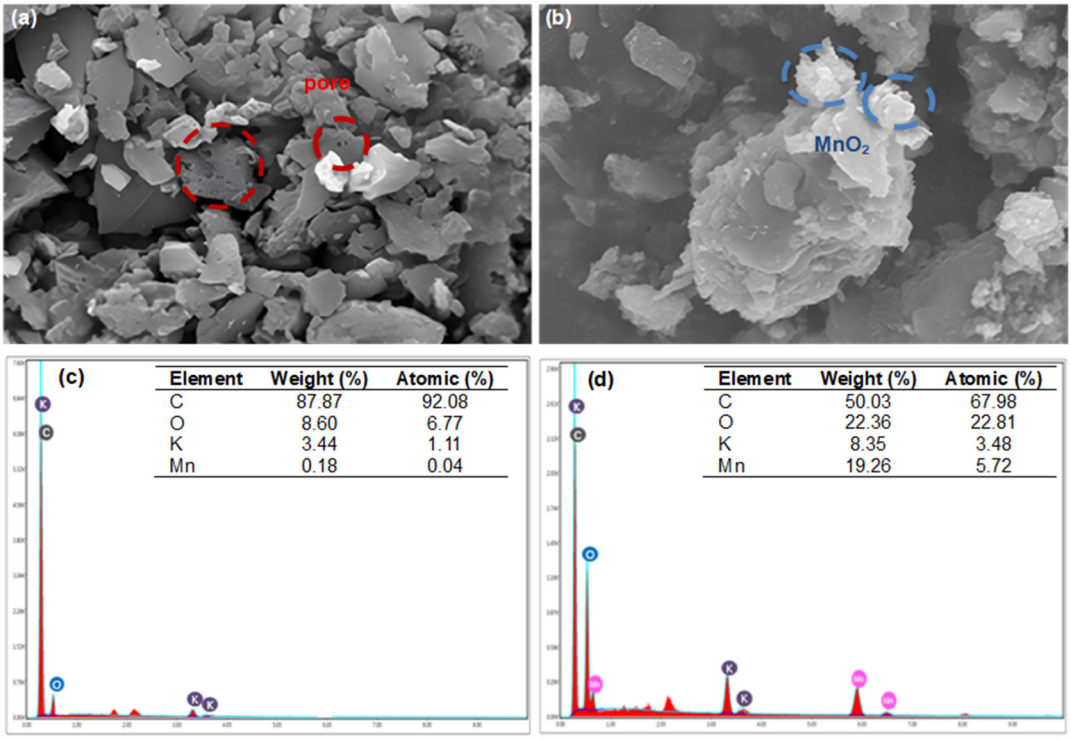

Fig 1. Morphological structure of the materials: (a) AC-PKS, (b) AC-PKS/MnO_2, and EDX mapping of the materials: (c) AC-PKS, (d) AC-PKS/MnO_2

by Pam et al. [12], pore structure growth occurs due to the activation process and thermal expansion during carbonization. This unique porous surface morphology is highly suitable for electrical storage, as it facilitates the diffusion of ions or molecules into the pore structure [21].

Fig. 1(b) shows the morphological structure of the surface of the AC-PKS/MnO_2 composite through the reduction reaction of $KMnO_4$ with AC. The result shows an increase in particle density and the presence of fine fibers on the surface of AC, which covers the pores of AC. Hamouda et al. [16] found that the morphology of the AC/MnO_2 composite consisted of thin, fiber-like nanowires bonded to AC from acacia wood. This was due to the influence of *in-situ* hydrothermal reactions on the AC surface, which can affect electrochemical performance. Wang et al. [19] also found something similar in their research, namely the morphology of the MnO_2/EC composite, which resembles thin fibers attached to the EC sheet. This shows that MnO_2 has been deposited on the surface of AC. The interface contacts between AC and MnO_2 will facilitate charge transfer and enhance the performance of the supercapacitor electrode.

Fig. 1(c) and 1(d) present the spectrum and elemental composition of the EDX analysis result. This analysis was conducted to identify the elemental composition and observe changes in composition after the composite was formed. Fig. 1(c) shows the EDX analysis of the AC-PKS sample, which has a composition of 87.78% C, 8.6% O, 3.44% K, and 0.18% Mn. The elements O and K appear due to the influence of activation using KOH. The Mn element composition in the AC-PKS sample was found to be 0.18% with an atomic weight of 0.04%, which can be considered negligible due to its very low concentration, as it may originate from the raw PKS or contamination. Fig. 1(d) shows the EDX analysis results of the AC-PKS/MnO_2 composite, indicating a decrease in the C composition to 50.03% and an increase in the Mn composition to 19.26%. The increase in Mn composition indicates that the AC-PKS/MnO_2 composite was successfully produced through the reduction reaction of $KMnO_4$ and is expected to be beneficial in electrochemical applications for energy storage [25].

Surface area and pore distribution measurements were performed using the Brunauer-Emmett-Teller (BET) method. Table 1 shows the specific surface area, pore volume, and pore size of both materials, namely AC-PKS and AC-PKS/MnO_2. Surface area measurements indicate that AC-PKS has a larger surface area and pore volume, specifically 960.79 m^2/g and 0.73 m^3/g, respectively, compared to AC-PKS/MnO_2, which have surface areas of 445.25 m^2/g and pore volumes of 0.40 cm^3/g. However, the pore size increased, specifically in AC-PKS by 3.04 nm, and further increased to 3.62 nm in AC-PKS/MnO_2. Choi et al. succeeded in synthesizing AC with a larger surface area of 1844 m^2/g and a decrease in surface area in the AC/MnO_2 composite to 1017–1505 m^2/g [24].

The research conducted by Yumak aligns with this study, with results indicating a 50% decrease in surface area in the MnO_2/AC composite. However, in the research, H_3PO_4 was used as an activator m^2/gm^2/g, showing a surface area of 628.18 m^2/g for AC and 336.45 m^2/g for the MnO_2/H_3PO_4-AC composite. The decrease in surface area and pore volume indicates that MnO_2 nanoparticles have formed, thus covering the AC pores and falling within the mesoporous range, which facilitates the diffusion of electrolyte ions into the pores, allowing for high-performance electrochemistry [26]. The correlation between SEM-EDX and SAA shows that although the addition of metal oxides reduces the surface area, MnO_2 can increase the pseudocapacitance value. This is due to the electrochemical properties of MnO_2, which allows it to provide capacitance values through redox reactions on the electrode surface, thus potentially improving electrochemical performance in supercapacitors [27].

Table 1. Surface area and pore characteristics of the AC-PKS and AC-PKS/MnO_2 composite

Sample	S_{BET} (m^2/g)	Pore volume (cm^3/g)	Pore size (nm)
AC-PKS	960.79	0.73	3.04
AC-PKS/MnO_2	445.25	0.40	3.62

Crystallographic Structure Analysis

XRD patterns were analyzed in the range of 2θ from 15° to 70°, to identify the crystal structure and phase of hydrothermal carbon from C-PKS, AC-PKS, and AC-PKS/MnO_2 composites are depicted in Fig. 2. The diffraction peaks in C-PKS show several prominent peaks at 22.3°, 44°, and 64.4°. The weak and broad peaks at 2θ = 22.3° corresponding to the (002) plane indicate an amorphous structure with low, irregular crystallinity [28]. Additionally, at 2θ = 44° and 64.4°, the peaks exhibit the general characteristics of carbon derived from hydrochar and resulting from the heating process of the raw sample. For AC-PKS, there is a sharp shift in the diffraction peaks from 22° to 26.7°, indicating the (002) crystal plane in the form of amorphous graphite due to activation and high temperature heating, followed by an increase in crystallinity at 44° and 64.4° [12,29]. Hafizah et al. [13] also obtained similar results, revealing an amorphous structure with diffraction peaks at (002) and (101) using the pyrolysis method. Meanwhile, in the study by Sevilla et al. [30], AC was successfully synthesized using the hydrothermal method with KOH as an activator and showed the same structure with broad but low-intensity diffraction peaks (002) and (100), as well as relatively good electronic conductivity, making it useful for electrochemical applications. These peaks indicate a microcrystalline structure and aromatic layers in the planar direction, thereby providing good electrical conductivity [29].

The diffraction pattern of the AC-PKS/MnO_2 composite shows new diffraction peaks at 2θ = 37.2° and 65.2°, corresponding to the (211) and (002) planes, respectively, as reported in JCPDS No. 44-0141 [17]. These characteristic peaks confirm the formation of the tetragonal nanoparticle phase of the α-MnO_2 type (JCPDS No. 44-0141) and δ-MnO_2 type (JCPDF No. 42-1317) [17,19]. The diffraction peak at 2θ = 43.9°, indicating the (100) plane, is characteristic of graphite carbon. The phase at this diffraction peak significantly contributes to the electrochemical process due to its good electrical conductivity [31]. After AC-PKS was reduced with $KMnO_4$, the peaks in the AC-PKS/MnO_2 composite exhibited peak broadening and a slight angle shift, indicating low crystallinity and the formation of an amorphous structure. Saini et al. [17] also conducted a similar study, demonstrating the formation of tetragonal α-MnO_2 nanoparticle phases with a diffraction peak at 37.6° in the (211) plane. Wang et al. [19] also found several diffraction peaks in the MnO_2/EC composite, namely 12°, 37°, and 65° with the (001), (111), and (020)

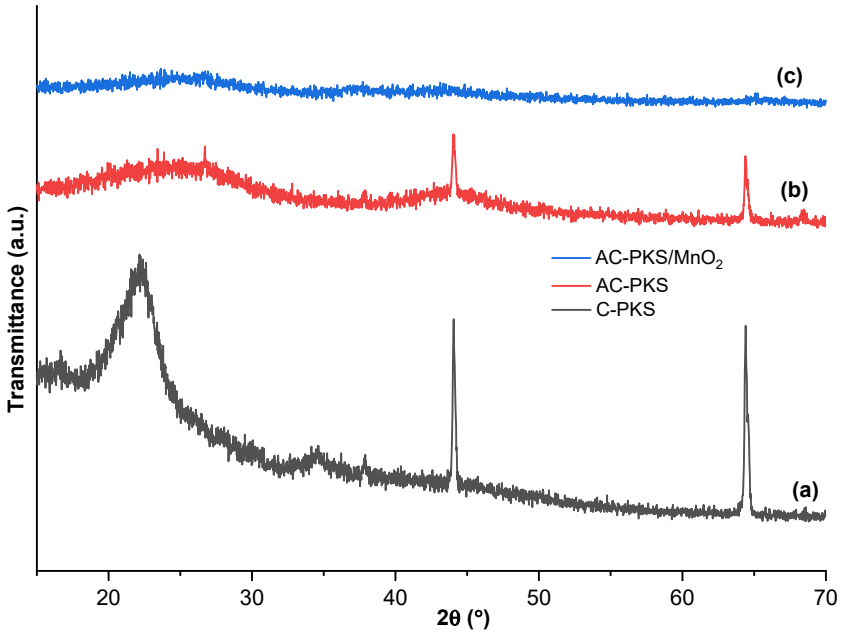

Fig 2. Diffraction pattern of C-PKS, AC-PKS, and AC-PKS/MnO_2 composite

planes of birnessite-type MnO_2 (JCPDF No. 42-1317). The amorphous diffraction peaks are highly suitable for supercapacitor applications, as they facilitate the reaction of electrolyte ions with a portion of the active electrode material, thereby enhancing the specific capacitance [25].

Functional Group Identification

Functional groups and structural or chemical changes in samples are analyzed using FTIR spectroscopy [32]. The spectra of three types of samples, namely C-PKS, AC-PKS, and AC-PKS/MnO_2 are depicted in Fig. 3. The FTIR spectra of C-PKS and AC-PKS show very significant changes in wavelength shifts and decreases in intensity. The broad peak at 3412 cm^{-1} indicates the presence of alcohol functional groups and water content [33]. In AC-PKS, the –OH group experiences a decrease in intensity and a peak shift to 3422 cm^{-1}, indicating the removal of some of the –OH groups during activation [34]. Additionally, the functional groups that appear in C-PKS and AC-PKS are C=O and C=C. In AC-PKS, the C=O and C=C functional groups are significantly reduced, as indicated by a decrease in intensity and a shift in wavelength, resulting in the chemical structure becoming that of an ester and an alkane, respectively. This decrease in intensity and a change in wavelength occur due to the activation process using KOH, which causes oxidation of the conjugated structure [35]. This transformation indicates that chemical activation effectively increases surface reactivity and porosity while modifying the original functional groups [30].

The AC-PKS/MnO_2 composite shows a new peak at a wavelength of 526 cm^{-1}, indicating the appearance of Mn–O bonds and the successful deposition of MnO_2 on the AC surface. Wang et al. [19] also found similar results at the Mn–O peak at 523 cm^{-1}. Hamouda et al. obtained an Mn–O peak at a wavelength of 499 cm^{-1} [16]. The –OH functional group remains visible, despite being weak, indicating the interaction between the remaining –OH groups on the surface and the MnO_2 particles formed during the $KMnO_4$ reduction process. The C=O groups were not detected in the composite samples, likely due to the reduction of $KMnO_4$ to MnO_2, causing the C=O groups to shift and stabilize as CO_2 in the range of ~2225–2500 cm^{-1} Combined with SEM-EDS, SAA, XRD, and FTIR analysis, the results indicate that MnO_2 has successfully been deposited onto the AC-PKS surface and has the potential to serve as an energy storage material.

Reduction of $KMnO_4$ Process for Composite AC-PKS/MnO_2

The reduction of $KMnO_4$ using AC-PKS as a reducing agent was analyzed using UV-vis spectroscopy. The reduction phase of $KMnO_4$ to MnO_2 was observed to

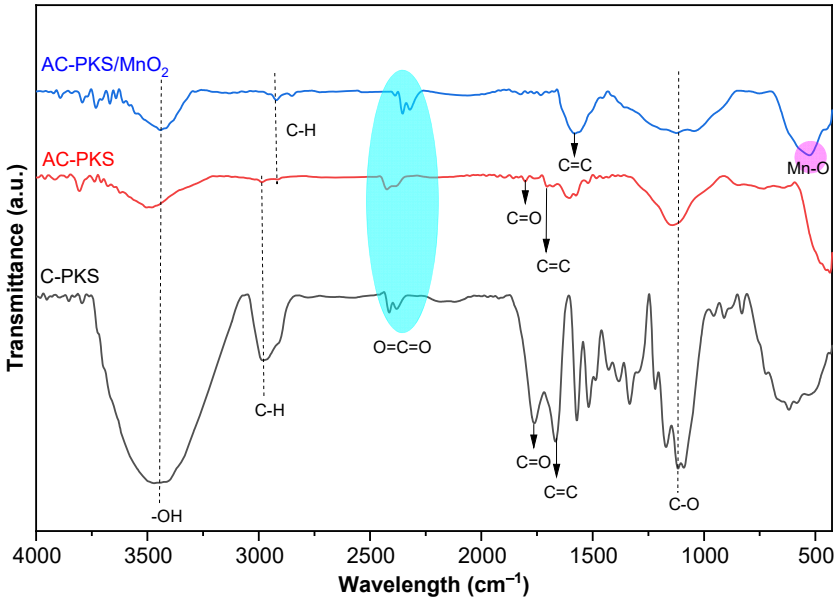

Fig 3. FTIR data of C-PKS, AC-PKS, and AC-PKS/MnO_2 composite

range from 1.5 to 7 h. The spectrum is shown in Fig. 4, with characteristic changes in absorbance indicating the transformation of Mn species during the reaction.

This spectrum shows changes in the absorption peaks that reflect the chemical transformation of $KMnO_4$ to MnO_2 and its interaction with AC. The sharp absorption peaks at 310, 525, and 545 nm are characteristic of MnO_4^- ions, which are purple and exhibit strong absorption at those wavelengths (Fig. 4). The absorbance peaks of $KMnO_4$ are at 312, 506, 525, 545, and 566 nm [36]. Over time, the intensity of these peaks decreases drastically, indicating that MnO_4^- ions undergo reduction. The decrease in the intensity of the 310 nm peak indicates that $KMnO_4$ has been complexed with AC, which acts as an efficient reductant in this reaction [37].

A new peak at 365 nm indicates the formation of a new species, specifically a MnO_2 or Mn^{4+} intermediate oxide, which shows the formation of MnO_2 nanoparticles in a colloidal form. As reported by Moon et al. [37], the characteristic peak of MnO_2 nanoparticles observed in the range of 360 to 404 nm is marked by a color change in the $KMnO_4$ solution from purple to brownish yellow. This spectroscopic observation is supported by the visual color change in the reaction solution shown in Fig. 5(a). This color transition is consistent with the loss of permanganate and the subsequent formation and precipitation of colloidal MnO_2.

Visual observation of the reaction solution provides additional support for the spectroscopic data. Fig. 5(b) illustrates the formation of a colloid produced by a laser beam directed at the bottle. There are significant Visual observation of the reaction solution provides additional support for the spectroscopic data. Fig. 5(b) illustrates the formation of a colloid produced by a laser beam directed at the bottle. There are significant differences marked by light scattering occurring in the three bottles. In bottle A (Fig. 5(b) (A)), there is no light scattering, indicating that there are no particles in the solution. The middle bottle, or bottle B (Fig. 5(b) (B)), displays the initial $KMnO_4$ solution with a characteristic dark purple color, consistent with the absorption peak at 310 nm, due to the presence of MnO_4^- ions. The right bottle, or bottle C (Fig. 5(b)–(c)), shows the reduced $KMnO_4$ solution with a brown color and turbidity, indicating the formation of MnO_2 in colloidal form [36-37]. This indicates the presence of the Tyndall effect from the scattered red laser light, which is evidence of the presence of colloidal particles in the solution.

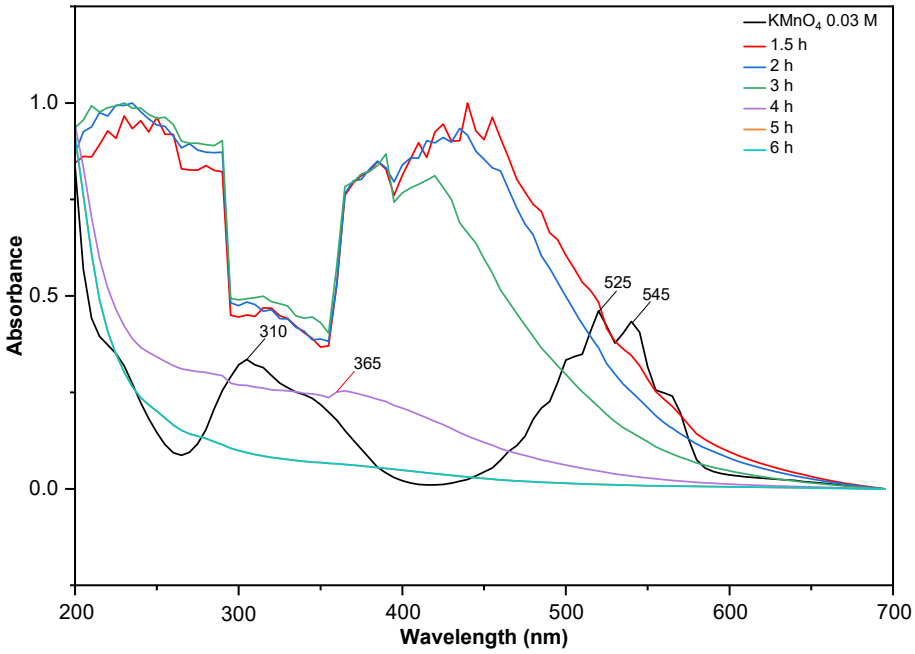

Fig 4. UV-vis absorption spectra of $KMnO_4$ solution with AC-PKS

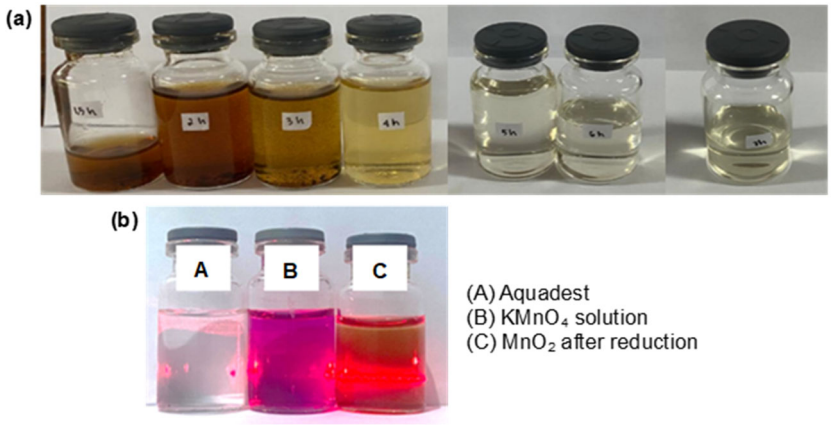

Fig 5. (a) Visualization of the reduction process of $KMnO_4$ to MnO_2 and (b) formation of MnO_2 colloid when fired with a laser beam

Electrochemical Analysis of the Electrode

The electrochemical performance of the electrode was analyzed using CV, GCD, and EIS with a 1 M H_2SO_4 electrolyte solution, as illustrated in Fig. 6(a). The tests were conducted in a voltage range of −0.2 to 0.8 V. Table 2 presents the results of measurements for C_{sc}, P_{sc}, and E_{sc} obtained from CV and GCD tests. The CV test results show that the C_s of the AC-PKS/MnO_2 composite increased compared to AC-PKS, from 23.32 to 67.85 F/g. This increase indicates that MnO_2 contributes to the pseudocapacitive properties of the electrode through reversible redox reactions between H^+ ions in the electrolyte and the MnO_2 surface. The pseudocapacitive properties of MnO_2 are influenced by ion exchange with the electrolyte, which causes redox reactions to occur with the electrolyte, as shown in Eq. (5) [38];

$$Mn_x(OH)^-_y + nH^+ + ne^- \leftrightarrow MnO_{x-n}(OH)^-_{y+n} \quad (5)$$

where $MnO_x(OH)^-_y$ and $MnO_{x-n}(OH)^-_{y+n}$ indicate higher and lower oxidation states, respectively, this reaction enhances the contribution to apparent capacity and is consistent with research conducted by Thuy et al. [22], which emphasizes the role of MnO_2 as an active material in redox-based supercapacitors using magnetic stirring and ultrasonic stirring methods, which obtained higher specific capacitance of 417 and 342 F/g, respectively. The CV curve in Fig. 6(b) shows a wider and more prominent area in the composite, indicating an increase in charge storage capacity and the pseudocapacitive properties of MnO_2, as shown by the quasi-rectangular curve shape [19]. These results are in line with the research conducted by Choi et al. [24], who obtained a specific capacitance of 60.3 F/g in AC/MnO_2 composites. Liu et al. [38] also obtained a lower specific capacitance of 42.73 F/cm^3 in AC fiber yarn/birnessite-type MnO_2 composites. Hamouda et al. [16] obtained a substantial specific capacitance of 301 F/g in AC from acacia wood/MnO_2 composites using the hydrothermal technique. Thuy et al. [22] stated that with a combination of AC and MnO_2, the apparent capacitance and electric double layer can be increased, due to the contribution of MnO_2. This shows that MnO_2 plays a vital role in increasing electrode capacitance and charge storage for supercapacitor applications [18,27].

GCD data support the increase in specific capacitance shown in Fig. 6(c), indicating that the AC-PKS/MnO_2 composite has a longer discharge time than the AC-PKS. This suggests that the energy storage capacity is higher. The increase in C_{sc} and P_{sc} is shown in Table 2. The C_{sc} increased from 32.65 to 46.91 F/g, and the P_{sc} from 4.53 to 6.51 W/kg. However, the E_{sc} showed a constant value of 250 Wh/kg. Hamouda et al. reported in their study that the AWPC/MnO_2 produced a higher power density of 450 W/kg, with an even distribution of MnO_2 on the surface of AC, forming nanowires [16]. Wang et al. also successfully synthesized δ-MnO_2 nanosheets on hierarchical porous carbon through a wet chemical reaction process, obtaining a high-power density of 500 W/kg with high conductivity [39]. The specific capacitance and power density found in this study

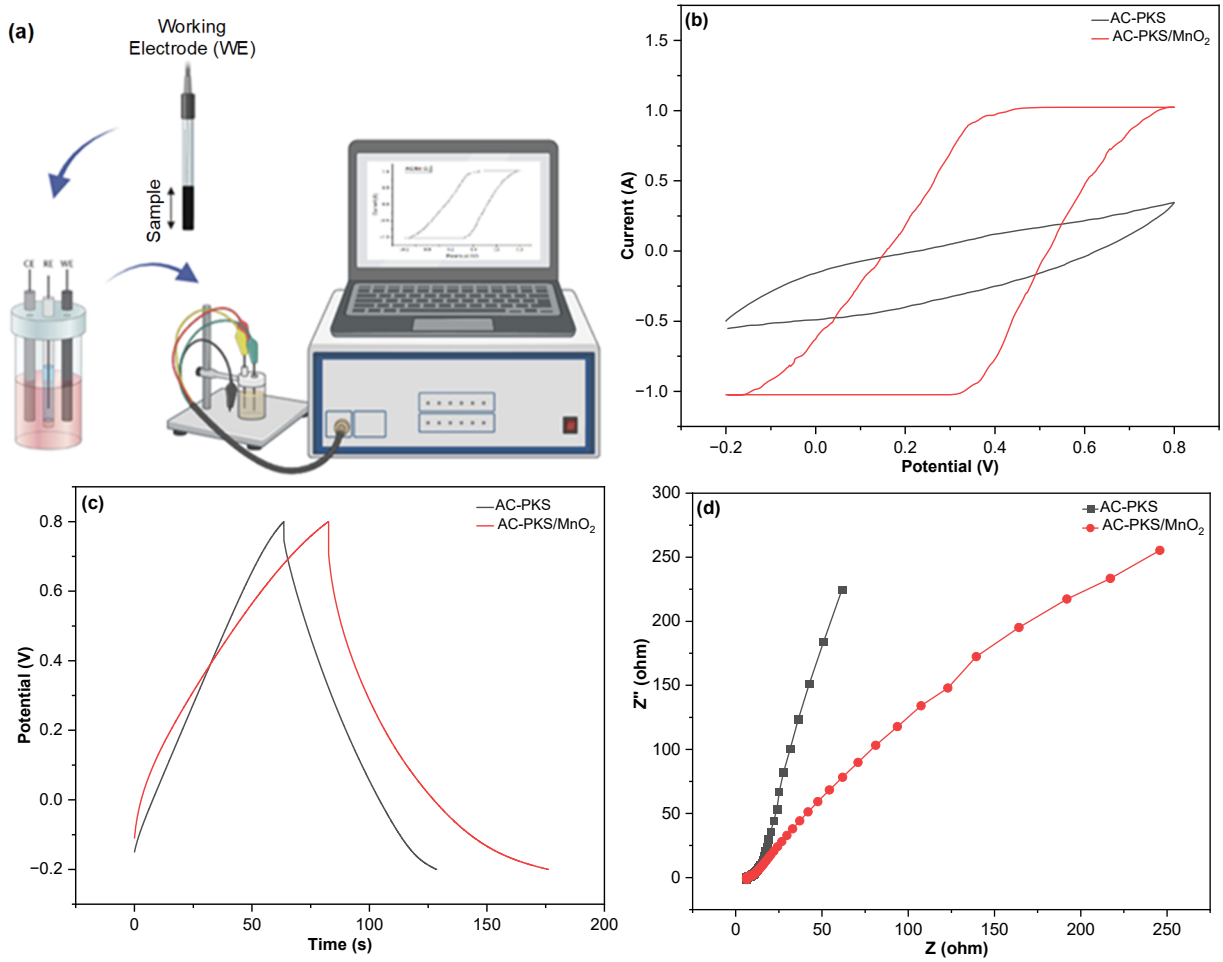

Fig 6. (a) Illustration of electrochemical testing of electrodes, (b) Voltammogram curve of CV, (c) GCD curve, and (d) Nyquist plot from EIS

Table 2. C_{sc}, P_{sc}, and E_{sc} of electrochemical testing of electrodes with CV and GCD

Sample	C_s (F/g)	C_{sc} (F/g)	P_{sc} (W/kg)	E_{sc} (Wh/kg)
AC-PKS	23.32	32.65	4.53	250
AC-PKS/MnO_2	67.85	46.91	6.51	250

still have a relatively low value, which can be due to the uneven distribution of MnO_2 on the AC surface, covering some of the pores of AC, thus limiting the diffusion of electrolyte ions and slowing down the charge transfer process. Additionally, the active mass of the electrode during the CV and GCD tests can also prevent the electrolyte from reacting completely with the electrode. Although the specific capacitance and power density values are still low compared to previous studies, the Nyquist plot from EIS (Fig. 6(d)) shows a decrease in internal resistance in the composite, indicating an increase in charge transfer efficiency. This indicates that the increase in charge transfer efficiency and electrode conductivity results in improved CV and GCD performance.

Overall, the results of this study show promising initial potential in the development of biomass-based electrode materials from PKS and MnO_2. The use of PKS biomass as an AC precursor offers both ecological and economic benefits. The integration of MnO_2 not only enhances electrochemical performance but also presents opportunities for application in green energy storage systems, utilizing a blue economy approach that prioritizes biomass waste. This research can be used as a reference for further exploration of pore structure

optimization, MnO_2 ratio and morphology, and more efficient synthesis techniques. With the right materials engineering approach, electrochemical performance can be significantly improved in terms of specific capacitance, power density, and energy density, thereby producing promising supercapacitor electrodes in the future.

■ CONCLUSION

This study successfully synthesized and characterized AC-PKS/MnO_2 composites through $KMnO_4$ reduction reactions, which showed significant potential for supercapacitor applications. FTIR analysis confirmed the formation of Mn-O functional groups at 526 cm^{-1}, while EDX showed the presence of Mn elements at 19.26%. XRD results revealed to the presence of MnO_2 on the surface of the AC, with diffraction peaks at 2θ = 37.2° and 65.2° SEM and SAA analysis revealed a porous morphology and mesopore size that support ion diffusion. The decrease in surface area indicates the presence of MnO_2, which can contribute to pseudocapacitance through a redox mechanism. Electrochemical testing using CV showed a threefold increase in specific capacitance from 23.32 to 67.85 F/g. This was supported by GCD testing, which showed an increase in specific capacitance from 32.65 to 46.91 F/g, accompanied by a longer discharge time in the composite. The Nyquist plot from the EIS test also shows a decrease in internal resistance in the composite, indicating an increase in charge transfer efficiency. Although the specific capacitance value produced is still not optimal, this research is a fundamental and promising preliminary study for the development of biomass-based electrode materials from PKS in energy storage systems. The results obtained open up opportunities for further exploration of pore structure optimization, MnO_2 ratio, and more efficient methods to achieve higher and sustainable supercapacitor performance, ultimately contributing to the development of future energy storage systems.

■ ACKNOWLEDGMENTS

The authors would also like to thank the Department of Chemistry, Faculty of Mathematics and Natural Sciences, Hasanuddin University, Indonesia, for providing science research and development laboratory, physical chemistry laboratory, and integrated laboratory facilities, as well as technical support during this research.

■ CONFLICT OF INTEREST

All authors affirm that there are no conflicts of interest associated with this article.

■ AUTHOR CONTRIBUTIONS

Ainun Rezkiva Arif wrote the manuscript and performed all the experiments. Muhammad Zakir and Ahyar Ahmad designed the research, developed the ideas, and coordinated the study. Indah Raya, Paulina Taba, and Herlina Rasyid contributed through validation of the research methodology, critical reviewing and editing of the manuscript. All authors have reviewed the final version of the work and agreed to the final version of this manuscript.

■ REFERENCES

[1] Dissanayake, K., and Kularatna-Abeywardana, D., 2024, A review of supercapacitors: Materials, technology, challenges, and renewable energy applications, *J. Energy Storage*, 96, 112563.

[2] Dar, M.A., Majid, S.R., Satgunam, M., Siva, C., Ansari, S., Arusalan, P., and Rafi Ahamed, S., 2024, Advancements in supercapacitor electrodes and perspectives for future energy storage technologies, *Int. J. Hydrogen Energy*, 70, 10–28.

[3] Zhang, J., Gu, M., and Chen, X., 2023, Supercapacitors for renewable energy applications: A review, *Micro Nano Eng.*, 21, 100229.

[4] Sharma, S., and Chand, P., 2023, Supercapacitor and electrochemical techniques: A brief review, *Results Chem.*, 5, 100885.

[5] Shah, S.S., Niaz, F., Ehsan, M.A., Das, H.T., Younas, M., Khan, A.S., Ur Rahman, H., Abu Nayem, S.M., Oyama, M., and Aziz, M.A., 2024, Advanced strategies in electrode engineering and nanomaterial modifications for supercapacitor performance enhancement: A comprehensive review, *J. Energy Storage*, 79, 110152.

[6] Nguyen, N.T.H., Tran, G.T., Nguyen, N.T.T., Nguyen, T.T.T., Nguyen, D.T.C., and Tran, T.V., 2023, A critical review on the biosynthesis,

properties, applications and future outlook of green MnO_2 nanoparticles, *Environ. Res.*, 231, 116262.

[7] Sivakumar, S., and Nelson Prabu, L., 2021, Synthesis and characterization of α-MnO_2 nanoparticles for supercapacitor application, *Mater. Today: Proc.*, 47, 52–55.

[8] Khalid, M.U., Zulfiqar, S., Khan, M.N., Shakir, I., Warsi, M.F., and Cochran, E.W., 2024, Electrochemical performance enhancement of MnO_2 nanowires through silver incorporation for next-generation supercapacitors, *Mater. Adv.*, 5 (15), 6170–6184.

[9] Zarshad, N., Rahman, A.U., Wu, J., Ali, A., Raziq, F., Han, L., Wang, P., Li, G., and Ni, H., 2021, Enhanced energy density and wide potential window for K incorporated MnO_2@carbon cloth supercapacitor, *Chem. Eng. J.*, 415, 128967.

[10] Kumar Mishra, R., Singh, B., and Acharya, B., 2024, A comprehensive review on activated carbon from pyrolysis of lignocellulosic biomass: An application for energy and the environment, *Carbon Resour. Convers.*, 7 (4), 100228.

[11] Gayathiri, M., Pulingam, T., Lee, K.T., and Sudesh, K., 2022, Activated carbon from biomass waste precursors: Factors affecting production and adsorption mechanism, *Chemosphere*, 294, 133764.

[12] Pam, A.A., Abdullah, A.H., Tan, Y.P., and Zainal, Z., 2022, Physicochemical properties of porous activated carbon prepared from palm kernel shell through a low-cost activation protocol, *S. Afr. J. Sci.*, 118 (9-10), 1–7.

[13] Hafizah, M.A.E., Manaf, A., Valency, T., Andreas, A., and Manawan, M., 2025, Optimized carbonization and kinetic analysis of palm kernel shell porous carbon for heavy metal adsorption, *Indones. J. Chem.*, 25 (3), 787–799.

[14] Che, C.A., and Heynderickx, P.M., 2024, Hydrothermal carbonization of plastic waste: A review of its potential in alternative energy applications, *Fuel Commun.*, 18, 100103.

[15] Abd Noor, S.A.M., and Al-Shamari, A.M.J., 2023, Preparation and performance of ZnO and ZnO/MnO_2 nanostructures as anode electrodes in DSSCs, *Indones. J. Chem.*, 23 (6), 1618–1626.

[16] Hamouda, H.A., Ramadan, A., Mokhtar, L.M., Ageeb, S.A., Ibrahim, M.H., Ajab, A.E., Hussein, M.B., Farah, A.A., Hassan, E.A., and Ma, G., 2024, Improving of the electrochemical performance of acacia wood porous carbon/MnO_2 nanocomposite as an advanced electrode for supercapacitor and oxygen evolution reaction, *Electrochim. Acta*, 495, 1444591.

[17] Saini, S., Chand, P., and Joshi, A., 2023, Electrochemical performance of MnO_2 composite with activated carbon for supercapacitor applications, *Indian J. Eng. Mater. Sci.*, 30 (3), 424–430.

[18] Tynan, B., Zhou, Y., Brown, S.A., Dai, L., Rider, A.N., and Wang, C.H., 2023, Structural supercapacitor electrodes for energy storage by electroless deposition of MnO_2 on carbon nanotube mats, *Compos. Sci. Technol.*, 238, 110016.

[19] Wang, X., Chu, J., Yan, H.J., and Zhang, H.K., 2022, Synthesis and characterization of MnO_2/eggplant carbon composite for enhanced supercapacitors, *Heliyon*, 8 (9), e10631.

[20] Nakason, K., Panyapinyopol, B., Kanokkantapong, V., Viriya-empikul, N., Kraithong, W., and Pavasant, P., 2017, Characteristics of hydrochar and liquid fraction from hydrothermal carbonization of cassava rhizome, *J. Energy Inst.*, 91 (2), 184–193.

[21] Li, J., Lin, Q., Wang, Z., Du, A., Luo, H., and Liu, Y.Q., 2023, Hierarchical porous carbon with high specific surface area and superb capacitance made from palm shells for supercapacitors, *Diamond Relat. Mater.*, 135, 109582.

[22] Thuy, L.T.T., Khu, L.V., and Lien, N.T.K., 2018, Synthesis, characterization and electrochemical performance of activated carbon supported MnO_2 for electrochemical capacitor, *Vietnam J. Sci. Technol.*, 56 (5), 582–593.

[23] Pedro Aguiar dos Santos, J., Cesar Rufino, F., Yutaka Ota, João I., Fernandes, R.C., Vicentini, R., Pagan, C.J.B., Morais Da Silva, L., and Zanin, H., 2023, Best practices for electrochemical characterization of supercapacitors, *J. Energy Chem.*, 80, 265–283.

[24] Choi, J.R., Lee, J.W., Yang, G., Heo, Y.J., and Park, S.J., 2020, Activated carbon/MnO_2 composites as electrode for high performance supercapacitors, *Catalysts*, 10 (2), 256.

[25] Liu, Y.H., Hsi, H.C., Li, K.C., and Hou, C.H., 2016, Electrodeposited manganese dioxide/activated carbon composite as a high-performance electrode material for capacitive deionization, *ACS Sustainable Chem. Eng.*, 4 (9), 4762–4770.

[26] Yumak, T., 2019, Electrochemical performance of fabricated supercapacitors using MnO_2/activated carbon electrodes, *Hacettepe J. Biol. Chem.*, 47 (1), 115–122.

[27] Liu, Y., Zuo, S., Shen, B., Wang, Y., and Xia, H., 2020, Fabrication of nanosized layered-MnO_2/activated carbon composites electrodes for high-performance supercapacitor, *Int. J. Electrochem. Sci.*, 15 (8), 7646–7662.

[28] Hasanah, M., Wijaya, A., Arsyad, F.S., Mohadi, R., and Lesbani, A., 2022, Preparation of hydrochar from *Salacca zalacca* peels by hydrothermal carbonization: study of adsorption on Congo red dyes and regeneration ability, *Sci. Technol. Indones.*, 7 (3), 372–378.

[29] Nasir, S., Hussein, M.Z., Zainal, Z., Yusof, N.A., and Mohd Zobir, S.A., 2018, Electrochemical energy storage potentials of waste biomass: Oil palm leaf and palm kernel shell-derived activated carbons, *Energies*, 11 (12), 3410.

[30] Sevilla, M., Ferrero, G.A., and Fuertes, A.B., 2017, Beyond KOH activation for the synthesis of superactivated carbons from hydrochar, *Carbon*, 114, 50–58.

[31] Sandeep, A., and Ravindra, A.V., 2024, Highly efficient peanut shell activated carbon via hydrothermal carbonization and chemical activation for energy storage applications, *Diamond Relat. Mater.*, 146, 111158.

[32] Gong, Y., Chen, X., and Wu, W., 2024, Application of Fourier transform infrared (FTIR) spectroscopy in sample preparation: Material characterization and mechanism investigation, *Adv. Sample Prep.*, 11, 100122.

[33] Kristianto, H., Susanti, R.F., Arie, A.A., Ondy, F.C., Chrismanto, C., and Devianto, H., 2020, Synthesis of activated carbon from salacca peel using hydrothermal carbonization and microwave assisted chemical activation as promising supercapacitor's electrode, *AIP Conf. Proc.*, 2255 (1), 060025.

[34] Rabichi, I., Ezzahi, K., Yaacoubi, F.E., Sekkouri, C., Bouzid, T., Ennaciri, K., Ounas, A., El Fels, L., Hafidi, M., Baçaoui, A., and Yaacoubi, A., 2025, Synthesis and application of biochar and KOH-activated carbon from olive mill solid waste for polyphenol removal, *J. Mol. Liq.*, 421, 126875.

[35] Yahia, E.H., Serafin, J., Román-Martínez, M.C., Sreńscek-Nazzal, J., Dziejarski, B., Saidi, M., and Ouzzine, M., 2025, Preparation of activated carbon from Moroccan argan press cake using KOH activation and its application for CO_2 adsorption, *Fuel*, 393, 134922.

[36] Sindhuja, M., Padmapriya, S., Sudha, V., and Harinipriya, S., 2019, Phase specific α-MnO_2 synthesis by microbial fuel cell for supercapacitor applications with simultaneous power generation, *Int. J. Hydrogen Energy*, 44 (11), 5389–5398.

[37] Moon, S.A., Salunke, B.K., Alkotaini, B., Sathiyamoorthi, E., and Kim, B.S., 2015, Biological synthesis of manganese dioxide nanoparticles by *Kalopanax pictus* plant extract, *IET Nanobiotechnol.*, 9 (4), 220–225.

[38] Liu, X., Zang, L., Xu, Y., Liu, Q., You, H., Chen, M., and Yang, C., 2021, Activated carbon fiber yarns with birnessite-type MnO_2 and oxygen-functional groups for high-performance flexible asymmetric supercapacitors, *Diamond Relat. Mater.*, 115, 108371.

[39] Wang, X., Chen, S., Li, D., Sun, S., Peng, Z., Komarneni, S., and Yang, D., 2018, Direct interfacial growth of MnO_2 nanostructure on hierarchically porous carbon for high-performance asymmetric supercapacitors, *ACS Sustainable Chem. Eng.*, 6 (1), 633–641.